Corrosion Science 184 (2021) 109378

Contents lists available at ScienceDirect

Corrosion Science

journal homepage: www.elsevier.com/locate/corsci

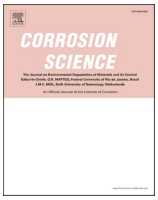

Short Communication

Self-generating construction of applicable corrosion-resistant surface structure of magnesium alloy

Ming Yin [a,c], Lifeng Hou [a,c,*], Zhiwei Wang [a,c], Tongyao Bao [a,c], Baosheng Liu [b], Huan Wei [a,c], Xiaoda Liu [a,c], Huayun Du [a,c], Yinghui Wei [a,b,c,*]

[a] College of Materials Science and Engineering, Taiyuan University of Technology, Taiyuan, 030024, Shanxi, China
[b] College of Materials Science and Engineering, Taiyuan University of Science and Technology, Taiyuan, 030024, Shanxi, China
[c] Corrosion and Protection Engineering Technology Research Center of Shanxi Province, Taiyuan, 030024, Shanxi, China

ARTICLE INFO

Keywords:
Replacement reaction
Mg-In alloy
Corrosion resistance
Corrosion layer

ABSTRACT

Magnesium alloys play a vital role in future development. However, the application of magnesium alloys with great potential is limited due to their strong corrosion sensitivity. In this work, the double-layer protective film of Mg-In alloy was constructed and adjusted by controlling the amount of indium (In) addition. The cross-section of the corrosion layer presents an inner In-rich layer accompanied by a compact outer layer of magnesium hydroxide with the distribution of Indium hydroxide alternating or interlayer, which significantly enhances the corrosion resistance of the Mg-In alloy and exhibits a self-generated function during the self-corrosion deposition process.

1. Introduction

Magnesium (Mg) and its alloys, as the lightest metal structural materials, have the potential to achieve lightweight products and reduce fuel consumption in the future [1–3]. However, a long-term obstacle to their application is vulnerability to corrosion, which curtails their shelf-life [4]. The main reason is that the corrosion products formed on the Mg surface is $Mg(OH)_2$, which is non-protective, and susceptible to the release of hydrogen when the Mg alloys encounter aqueous and/or corrosive media [5,6]. Customarily, mitigation methods include surface modification, for example, chemical conversion coating [7–9], electroplating [10], anodizing [11] and etc., alloying [12,13] and addition of inhibitors [14] to media. Admittedly, the addition of inhibitors is restricted by working conditions and the surrounding environment [14]. In addition, surface modification is considered to be an effective method, but it is restricted to a limited range of the surface. Even if the surface of the alloy is improved by some special methods, corrosion is inevitable once the coating is destroyed during operation. Even until now, Mg alloying and subsequent heat treatments are a priority solution to reduce the corrosion sensitivity. The main mechanisms can be described as the adjustment of microstructure [15,16] (change in volume fraction and distribution of the precipitates), sequester impurities [3], transformation of film density [17,18] and cathodic poisoning [19]. After comparison, there is a commonality between the Mg alloying method that changes the compactness of the corrosion layer and the surface modification, i.e., film formation hinders corrosion, while the latter may not reach the former in terms of improving corrosion resistance. However, the numerous advantages of alloying, such as the spontaneous generation of the layer and the absence of complex pre-treatment, have tempted many scholars [17,18] to conduct research on it. Hou et al. [18] studied the passivation and dissolution properties of corrosion-resistant Mg-33at.%Li alloy in chloride aqueous solution, and found that the addition of Li can restrict the kinetics of the anode reaction. Moreover, the surface enrichment of Li generated by alloy dissolution (mainly composed of sparingly soluble lithium carbonate) can protect the film from corrosion stably for a long time.

The method of constructing the corrosion layer structure deserves in-depth study. In the study of the characteristics of the film, many reports [20–24] have been found that Sn element in Mg-Sn alloys can be present in the film to increase the compactness of the layer. Some of them [21, 23] believe that the formation of a Sn-rich layer on the alloy surface will inhibit cathode hydrogen evolution and reduce the corrosion rate significantly. Therefore, it is a commendable strategy to construct a new type of Mg alloys with self-passivation ability. However, the film formed by the addition of common elements does not provide better protection much less prevent the propagation of corrosion. Therefore, it is

* Corresponding authors at: College of Materials Science and Engineering, Taiyuan University of Technology, Taiyuan, 030024, Shanxi, China.
E-mail addresses: houlifeng78@126.com (L. Hou), yhwei_tyut@126.com (Y. Wei).

https://doi.org/10.1016/j.corsci.2021.109378
Received 15 October 2020; Received in revised form 2 March 2021; Accepted 7 March 2021
Available online 10 March 2021
0010-938X/

necessary to design a dense and controllable corrosion protection layer structure. To achieve this effect, alloying was used to build a double-layer protective film structure that inhibits corrosion propagation. It is conceivable that the selected additives must have a suitable solid solubility, and be noble than Mg without introducing a second phase [25]. Therefore, a lot of attempts have been made, and alloying elements with this adjustment function have been selected. Indium (In), which stands out among many alloying elements, was chosen to develop a new type of corrosion-resistant Mg alloy. However, few studies on the corrosion resistance of In to Mg have been reported, and most of the literature focuses on the discharge behavior of In to Mg [26–29]. It is noteworthy that these studies on the discharge behavior are based on Mg-Al alloys, making the behavior of In to Mg complex. Studies on the corrosion resistance of In to Mg have focused on the effect of noble metal elements on Mg [30]. For example, Gore et al. [30] studied the enrichment efficiency of noble metal elements on magnesium and effect on hydrogen evolution, and concluded that Mg-0.1 wt.% In alloy shows high cathodic activation efficiencies. And here the impurity properties were shown by the low In concentration. However, when higher In concentrations were studied, we found that In does not act as an impurity like Fe, but has the effect of optimizing the corrosion layer structure. To this end, various reasonable addition concentrations were designed, and three typical alloys (Mg-xIn, x = 0.5, 1, and 2 wt.%, specific compositions are shown in Table S1.) were chosen for illustration. Solution treatment was used to homogenize the Mg-In alloys, which helps In to diffuse sufficiently in the Mg matrix without differences in the alloy composition.

2. Materials and methods

2.1. Sample preparation

A series of as-cast Mg-xIn (x = 0, 0.5, 1, and 2 wt.%) alloys were designed with nominal components consisting of commercial pure Mg (≥ 99.99 %) and pure In (≥ 99.99 %). They were smelted in a PDM-1 type-inclined Mg-alloy furnace protected by a mixed gas (99.7 % CO_2 + 0.3 % SF_6). First, a stainless steel crucible containing pure Mg was placed in the furnace with the temperature raised to 720 °C for a period of time. Next, the addition of indium was carried out after the melting of pure Mg. Then, the contents were stirred and the slag was removed after 30 min of static. The melt was poured into a right-angled stainless steel mold to obtain as-cast Mg-In alloy ingots. To eliminate dendrite segregation and to make the In dissolved completely in the α-Mg matrix, it was chosen to be incubated at 450 °C for 24 h and quenched with water. The specific compositions of the studied alloys were analysed via inductively coupled plasma-atomic emission spectroscopy (ICP-AES, Optima 7000DV), and the results are listed in Table S1. The materials used in the control samples were commercial die-cast AZ31B and AZ91D Mg alloys. The ingots were cut into coupons (15 mm × 15 mm × 5 mm) and polished using a series of silicon carbide papers (180, 400, 600, 1000, and 2000 grit) and ultrasonically washed with anhydrous ethanol for follow-up studies. All studied alloys were taken from surfaces of the same orientation in the same position.

2.2. Microstructural characterization

X-ray diffraction (XRD, TD-3500) was used to accurately identify the processed corrosion products (comprising collection, cleaning, drying and grinding) after long-term immersion (100 days). The test parameters were as follows: Cu K_α radiation target was used, the scanning speed was 2°/min, and the scanning angle was 20° to 80°. The characterization of the cross-sectional morphologies of the specimens were observed by scanning electron microscopy (SEM, TESCANVEGA3). The accelerating voltage of SEM was 20 kV. Elemental content analysis of the specimens was obtained using the micro-area composition of an energy-dispersive X-ray spectroscopy (EDS, Oxford). Macroscopic morphologies of corrosion were photographed with a SLR camera model Canon EOS-200D. An X-ray photoelectron spectroscopy (XPS, ESCALAB 250) was used to examine the chemical composition of the corrosion products (comprising collection, cleaning, drying and grinding). Measurements were performed using the indeterminate C_{1s} signal, which was set at 284.6 eV to correct all the binding energy values in the XPS spectrum. XPSPEAK 4.1 software was used to analyze the results. Corrosion layer structure was characterized and identified using focused ion beam (FIB, FEI Helios Nanolab 600) and transmission electron microscopy (TEM, JEM-ARM200 F).

2.3. Electrochemical test

Potentiodynamic polarization curves were measured using an electrochemical workstation (SP-150, Bio-logic Science Instruments, France) equipped with a standard three-electrode cell. Sample coupons with an exposed area of 1 cm^2 were used as working electrodes, a saturated calomel electrode (SCE) as reference electrode and platinum mesh as counter electrode. A solution (pH 6.8–7.2) of 0.6 M NaCl prepared with reagent-grade sodium chloride and deionized water for electrochemical testing. Electrolyte temperature was controlled using a water bath equipped with a thermostat, and all the experiments were performed at the temperature of 25 ± 2 °C. Prior to the polarization curve tests, the working electrode must be immersed in the electrolyte for 15 min to ensure that the surface of alloy is in a stable state. Polarization curves were recorded at a scan rate of 1 mV/s with a scan range of −200 mV/Ecorr to +500 mV/Ecorr. Since the anode branch is strongly affected by the formed corrosion products and is not under activation control for the charge transfer, the cross-section of cathodic slope with the E_{corr} was used instead of the Tafel extrapolation method to fit the data.

2.4. Immersion experiments

The specimens used for mass loss measurements and immersion experiments were exposed in a solution of 0.6 M NaCl for various times at room temperature. The corrosion behavior of the investigated alloys was evaluated periodically. The ratio of the immersed sample contact area (in cm^2) to the 0.6 M NaCl solution (in mL) was 1:200 to ensure that the immersion test was not affected by changes in pH. Corrosion products were dissolved by immersion in an aqueous solution of chromic acid (200 g/L of CrO_3 + 10 g/L of $AgNO_3$), abiding by the ASTM G1 standard. Samples immersed for 5 days were selected for mass loss measurements and weighed with a highly accurate digital balance (AL204-IC, Mettler Toledo). Hydrogen gas was collected periodically using a combination of an inverted funnel and burette. The samples used for hydrogen evolution test were ground to 2000 grit, and the exposure area of the test samples in 0.6 M NaCl solution was 1 cm^2. The effect of scratches on the In-rich layer and the dense oxide layer was explored by artificially destroying the surface of the Mg-2In alloy that had been corroded. The corroded alloy surface (samples that had been immersed in 0.6 M NaCl solution for 120 days) was scratched by a sharp ceramic knife, and then immersed in 0.6 M NaCl solution for 100 days. All experiments were performed in triplicate to provide confidence and accuracy of the results.

3. Results and discussion

To show the remarkable superiority of corrosion resistance of the studied alloys, typical Mg alloys [3,16,31–34] and pure Mg immersed in the same concentration of NaCl solution were selected for comparison. In regards to the corrosion rates measured upon Mg alloys, the available i_{corr} data fitted from polarization curves under certain conditions are of wide applicability. Fig. 1a shows a comparison of the potentiodynamic polarization curves of typical Mg alloys and pure Mg. Obviously, the cathodic kinetics of Mg-In alloy are reduced significantly relative to

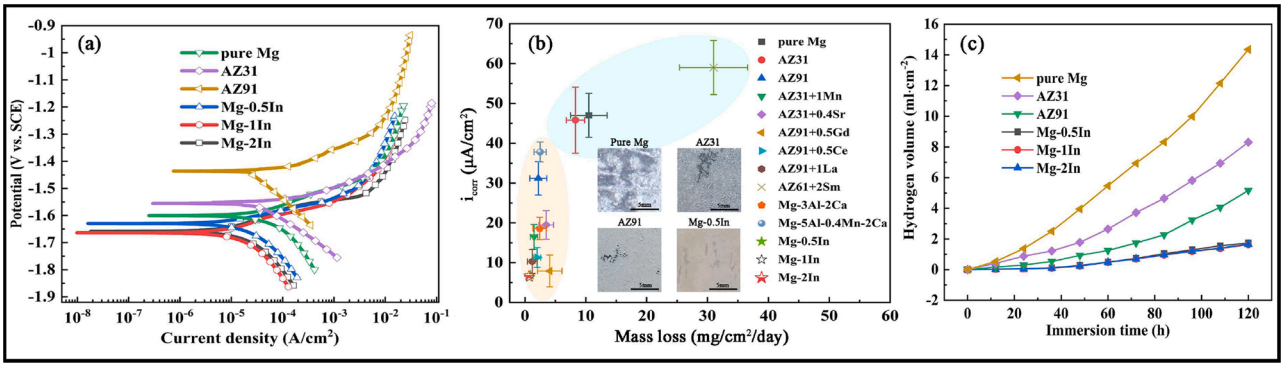

Fig. 1. A rough comprehensive evaluation of corrosion behavior: (a) Comparison of potentiodynamic polarization curves of typical alloys. (b) Corrosion rate expressed as corrosion current density (i_{corr}) versus mass loss rate [3,16,31–34] (mass loss determined in 0.6 M NaCl). (c) Hydrogen volume for various samples immersed in 0.6 M NaCl at OCP for 5 days.

AZ31 and pure Mg, with no concomitant change in anodic kinetics. For a more pronounced contrast effect, the corrosion rate, expressed as corrosion current density (i_{corr}) versus mass loss rate, is shown in Fig. 1b. The corrosion resistance of Mg-xIn (x = 0.5, 1 and 2 wt. %) alloys is significantly higher compared to typical Mg alloys and pure Mg. The corrosion morphologies of the four samples immersed in the solution of 0.6 M NaCl for 20 h are shown in the illustrations. The remarkable corrosion resistance of the Mg-0.5In alloy (the weakest degree of corrosion) was further verified by corrosion morphology (insert in Fig. 1b). In addition, Fig. 1c also gives the volume of hydrogen collected from various samples immersed in 0.6 M NaCl for 5 days under natural conditions to assess the reliability of corrosion resistance. The volume of hydrogen collected of the Mg-In alloys is much lower than that of the control alloys, which indicates that the addition of In can greatly inhibit the hydrogen evolution rate of the Mg alloy.

The distinguishing results of a clear corrosion layer structure are revealed by comparing the interface structure of pure Mg and Mg-In alloys. The penetration effect of the corrosive solution cannot be prevented due to the presence of a loose corrosion layer structure on the pure Mg surface (Fig. 2a). However, the formation of a dense double-layer protective structure consisting of corrosion products and In-rich layer acts to block or retard the penetration of corrosive solution (Fig. 2b). This is completely consistent with the results of the above-mentioned evaluation of the difference in corrosion performance. A line scanning of the white substance adjacent to the interface between the Mg-0.5In matrix and the corrosion layer results in a clear distribution of In concentration fluctuations (a distinctly elevated In concentration in the range of about 3 μm of the In distribution in the inset of Fig. 2b), indicating that the white substance is the aggregation of substances containing indium elements (In species). The concentration of In addition affects the formation and sequencing of the structure of the corrosion products. It is the combination of an inner In-rich layer and a compact outer corrosion products, as for the Mg-In alloy mentioned in this study. However, with increasing In concentration, the cross-section of the corrosion layer presents an inner In-rich layer accompanied by a compact outer corrosion products layer with magnesium hydroxide and reticulated distribution of In-containing substances (Fig. 2c). The cross-section of the outer corrosion layer of the Mg-1In alloy also presents the distribution of In species alternating or interlayer (Fig. 2d). The appearance of this structure is related to the migration conditions of In species [35–37]. This migration process of In atoms apparently occurs by diffusion. Stokes-Einstein (SE) relation ($D = \frac{RT}{6L\pi r\eta}$), which predicts this size-dependent mobility (self-diffusion coefficient D), where R is the molar gas constant, T is the absolute temperature, L is the Avogadro constant, η is the viscosity, and r is the particle radius. Excess accumulated In species could not migrate to the interior of the corrosion layer concurrently, which causes the In species remaining in the corrosion layer. Conversely, the less accumulated In species have good migration properties. In this case, In species (mainly metallic In, which will be described below) well aggregated and formed an In-rich layer at the boundary between the corrosion layer and the matrix. The aggregation of these In species indicates that In element has undergone spontaneous migration and tended to aggregate itself. To ascertain the presence of In species embedded in the $Mg(OH)_2$ film, a line scan (Fig. 2f) was performed on a typical location in the $Mg(OH)_2$ film of the Mg-2In alloy (Fig. 2e). Thus, it was confirmed that the white substance embedded in the $Mg(OH)_2$ film was identified as the In species. The In species are distributed in the interstices of the loose $Mg(OH)_2$ (white strips or dots in the Fig. 2e). Afterwards, the corrosion layer was subjected to scratching treatment to evaluate the self-healing ability of the double-layer protective film structure. The artificially damaged samples exhibited devastating damage (Fig. 2g), but after a long-term self-repairing, stronger and more efficient corrosion layer reconstruction results (Fig. 2h) are shown in cross-sectional morphology. The reconstruction mechanism and effect of this film is completely different from other surface modifications. In contrast to many other surface modifications, the self-repairing function of this complete structure regeneration is formed spontaneously at any time without being restricted by the degree of damage. Moreover, it is not restricted by complicated pre-processing.

The corrosion products were tested by XRD to verify the composition of the corrosion layer structure, and only the $Mg(OH)_2$ was detected (Fig. 3a). To accurately determine the double-layer protective film, the processed corrosion layer (comprising collection, cleaning, drying and grinding) was subjected to XPS inspection due to the limitation of XRD detection. Fig. 3b shows the decomposition-fitted curve of XPS spectrum of the In3d. By peak fitting and comparison with the standard binding energy, the high-resolution spectrum of $In3d_{5/2}$ can be decomposed into a characteristic peak of metallic In with binding energy of 443.6 eV and a characteristic peak of $In(OH)_3$ with binding energy of 445.1 eV. In the case of such a low binding energy, only the presence of metallic In can be confirmed. The presence of metallic In in the corrosion products confirms that the dissolved In^{3+} have undergone a reduction process. To further determine the composition distribution of the corrosion layer structure, long-term processed samples (immersed in 0.6 M NaCl solution for 300 days) were subjected to FIB for TEM observation. The reasonable sampling boundary, sampling location and test area information are shown in Fig. S1. Aggregation and non-uniformity of elements in the test area of Mg-1In alloy were revealed clearly in the elemental distribution maps (Fig. 3(e–g)). Metallic In undoubtedly exists in the inner In-rich layer by the combination of XPS and TEM identification. To explore the generation of this structure, the following discussion is proposed.

The *in situ* self-generating double-layer protective film, consisting of inner metallic layer and outer alternating and reticulated double-layer protective film, constructed by alloying method is of great significance for Mg alloys. The formation mechanism of this double-layer protective

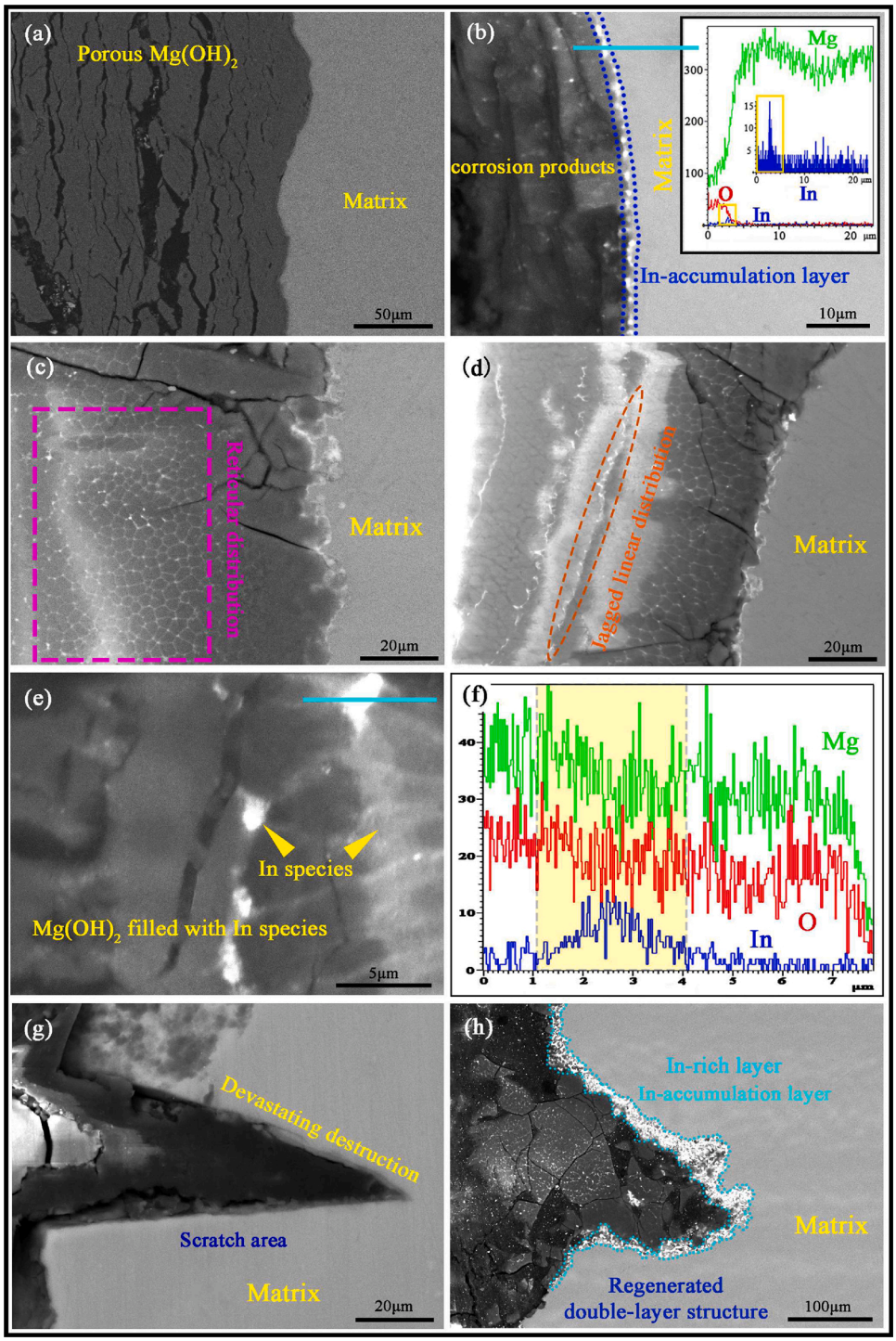

Fig. 2. Cross-section morphologies. (a) SE image of pure Mg (immersed in 0.6 M NaCl for 3 days). (b) Mg-1In alloy (immersed in 0.6 M NaCl for 25 days). (c) and (d) Mg-1In alloy (immersed in 0.6 M NaCl for 200 days). (e) Corrosion layer of Mg-2In alloy. (f) line scanning of the study area of (e). (g) The morphologies of the corroded Mg-2In alloy specimen (samples that had been immersed in 0.6 M NaCl solution for 120 days) after being scratched. (h) 100 days after re-immersion in 0.6 M NaCl solution.

film was proposed by the following illustration and the above-mentioned verification. The cross-sectional mechanism diagram of the relevant reactions during corrosion of Mg-In alloys are clearly depicted in Fig. 4. The alloy was inevitably dissolved when the alloy was placed in a solution of 0.6 M NaCl (Fig. 4a). According to Akimov theory [38,39], the anodic dissolution of the matrix will lead to the disintegration of the crystals of the solid solution. Mg spontaneously loses electrons to form Mg^{2+} (reaction ① in Fig. 4a), and then In in the Mg lattices loses electrons to form In^{3+} (reaction ② in Fig. 4a). At the same time, the hydrogen generated by the combination of the lost electrons with H^+ ions (reaction ③ in Fig. 4a). Once In^{3+} is dissolved in the solution, the replacement reaction [27] (reaction ④ in Fig. 4a) is spontaneously generated by the metals' standard potentials [40] as a driving force. The resulting In atoms will be firmly deposited on the surface of Mg particles, as evidenced by Gore et al. [41]. As the replacement reaction proceeds, the Mg atoms on the surface are gradually replaced by the generated In atoms, thereby forming an In-rich layer. The dissolved Mg^{2+} combines with OH^- to form a $Mg(OH)_2$ film (reaction ⑤ in Fig. 4a) distributed outside the In-rich layer. In-rich layer occupies the reactive sites of alloy surface, thereby retarding the dissolution of the alloy surface. $In(OH)_3$, formed by the combination of In^{3+} and OH^- (reaction ⑥ in Fig. 4a), partially enters into the voids of porous $Mg(OH)_2$ film. The formation of In-rich layer and compact $Mg(OH)_2$ film retards the dissolution of the alloy surface (Fig. 4b). Consequently, the corrosion resistance of the

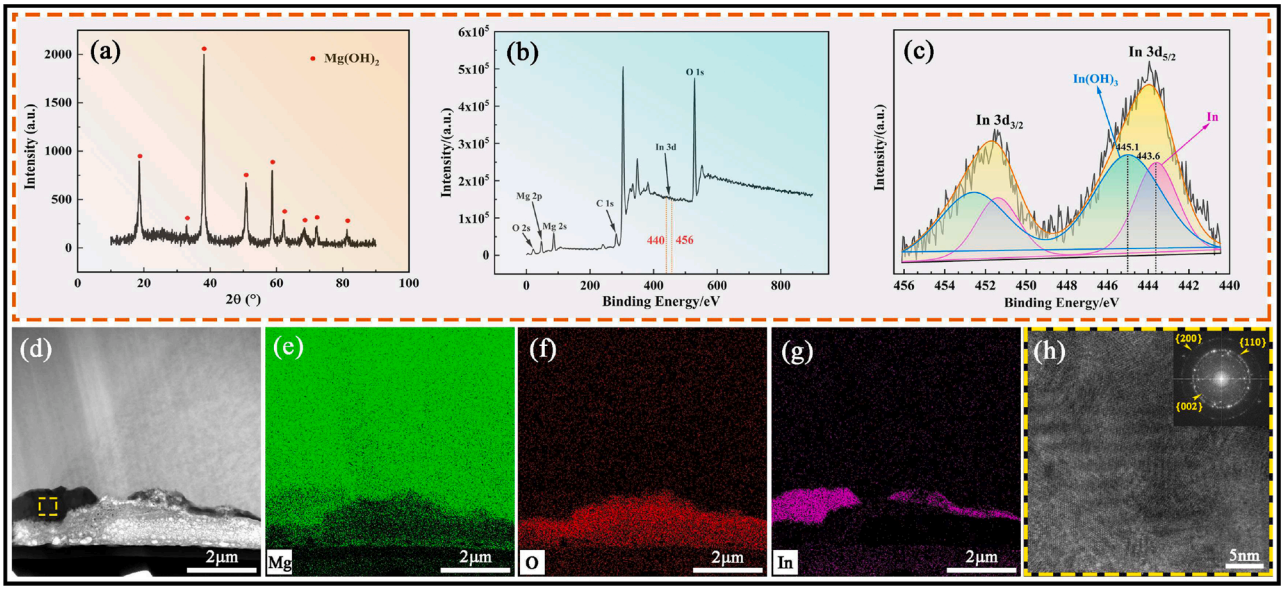

Fig. 3. Characterization results of corrosion products of Mg-1In alloys immersed in 0.6 M NaCl for 200 days. (a) XRD pattern. XPS spectra characteristics of the wide XPS spectrum (b) and In3d peak (c). (d) TEM image of cross-section morphology. (e), (f), and (g) are the element distribution maps of Mg, O, and In in (d), respectively. (h) High resolution TEM image and the corresponding selected area diffraction pattern (SADP) of the dotted area in (d).

Mg-In alloys are enhanced drastically. Notably, the In particle seem to has a great galvanic effect with the Mg matrix and accelerate the corrosion rate of Mg. However, this is different from the corrosion of impurities such as Fe affecting pure Mg. In the initial stage of corrosion, it is difficult for the metallic In produced by replacement reaction to gather together in a short time to form larger In particle. It is worth noting that the formation of In particles takes some time, rather than immediately forming a stronger galvanic effect. The traces of metallic In formed by short-term corrosion hardly produce a galvanic effect. Even if metallic In is formed, it is dispersed fine particles that do not exert a significant galvanic effect. With time, even if very fine particles form agglomerated metallic In by diffusion, the surface of Mg-In alloys has been covered by corrosion products. Some In particles are distributed in the corrosion products and others are enriched between the matrix and the corrosion layer. The dense corrosion layer acts as a better barrier and significantly slows down the ability of the corrosion medium to penetrate. Therefore, metallic In does not form a great galvanic effect.

Over time, $Mg(OH)_2$ still cannot prevent the penetration of the corrosive medium in some loose parts, and the deviation of the longitudinal corrosion appeared. The relevant mechanism of long-term immersion is shown in Fig. 4c. Obviously, the deeper the corrosion progresses, the more In species aggregates (including $In(OH)_3$ and metallic In) can be detected. The metallic In present on the surface of In species aggregates is inevitably oxidized to $In(OH)_3$. The presence of larger In species aggregates on the alloy surface allows the corrosion proceed selectively to the more susceptible areas (weak areas). The long-term corrosion causes the In species aggregates to stay in the corrosion layer and play a role in filling. The permeation channel of the corrosive medium was occupied by metallic In (and then oxidized to $In(OH)_3$) generated by the replacement reaction, presenting a network structure filled with regular In species. The striped In-rich layer is retained in the film due to the further progress of corrosion. The structure of the corrosion layer under long-term immersion is a compact outer corrosion layer with the distribution of In species alternating or interlayer/In-rich layer/matrix. To verify the superiority of this double-layer corrosion layer structure, the corrosion layer of alloys immersed in 0.6 M NaCl for a long time was observed and evaluated periodically. The superiority of the corrosion layer structure in inhibiting corrosion propagation was reflected by monitoring the thickness of the alloys corrosion layer regularly (Table S2). It is worth noting that the corrosion resistance of the Mg-In alloy depends on the compactness of the outer corrosion layer filled by In species and the continuity of the inner In-layer. For this paper, when the In concentration reaches 0.5 wt.%, both the compactness of the peripheral corrosion layer and the inner In-layer achieve a good protection. When the In concentration continues to increase (e.g., Mg-1In and Mg-2In), the compactness of the corrosion layer and the continuity of the In-layer will only be slightly enhanced. Essentially there are no other mutating factors for corrosion resistance. Therefore, no significant change in corrosion resistance occurs with increasing In concentration to some extent. It is possible that the corrosion resistance changes when the In concentration increases significantly, e.g., when the In concentration reaches 10 wt.%, 20 wt.% or higher, but this is beyond the scope of this paper. The above mechanism is completely consistent with the phenomena that occur during the observation and research, so the mechanism proposed in this paper is logical.

4. Conclusions

In summary, a substantial breakthrough has been made in the construction of a new type of Mg alloy interface structure. The formed double-layer protective film structure dramatically enhances the corrosion resistance of the Mg-In alloy. The cross-section of the corrosion layer presents an inner In-rich layer accompanied by a compact outer corrosion layer with the distribution of In species alternating or interlayer, even if this structure is not continuous across the interface of the sample. This corrosion layer exhibits a self-generated control function during the self-corrosion deposition process. Moreover, even with scratching and abrasion, the effect of this self-repairing double protective layer is still effective.

Data availability

The raw/processed data required to reproduce these findings cannot be shared at this time as the data also forms part of an ongoing study.

CRediT authorship contribution statement

Ming Yin: Methodology, Conceptualization, Formal analysis, Investigation, Writing - original draft, Writing - review & editing. **Lifeng Hou:** Conceptualization, Writing - review & editing, Funding

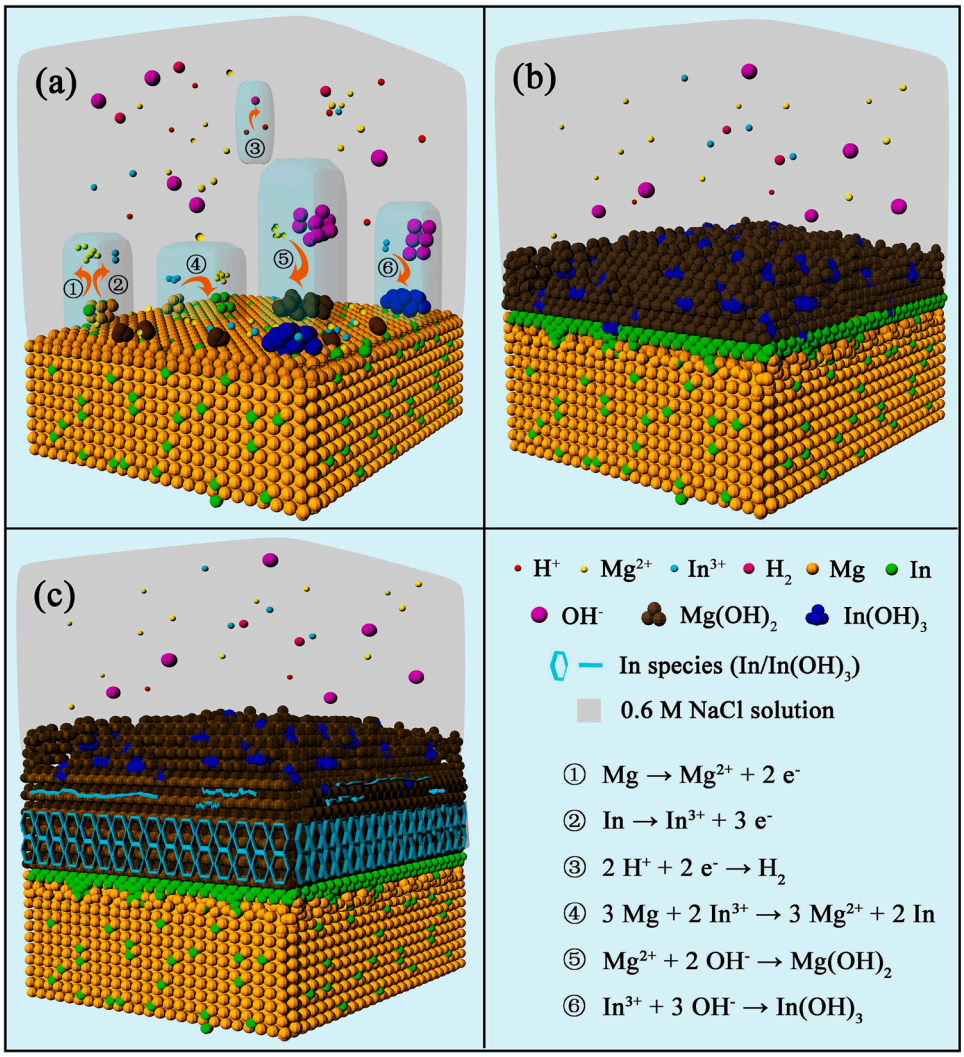

Fig. 4. Schematic diagram of the cross-sectional mechanism of galvanic replacement reaction during corrosion of Mg-In alloys: (a) Corrosion process such as adsorption and replacement reaction of In ions on Mg surface. (b) Corrosion layer formed after a short period (25 days) immersion. (c) Corrosion layer formed after long period (200 days) immersion.

acquisition. **Zhiwei Wang:** Methodology, Investigation, Writing - review & editing. **Tongyao Bao:** Methodology, Writing - review & editing. **Baosheng Liu:** Methodology, Writing - review & editing. **Huan Wei:** Formal analysis, Writing - review & editing. **Xiaoda Liu:** Methodology, Investigation. **Huayun Du:** Investigation, Formal analysis. **Yinghui Wei:** Project administration, Funding acquisition, Writing - review & editing.

Declaration of Competing Interest

The authors declare no competing financial interest.

Acknowledgements

This work was supported by the National Natural Science Foundation of China (No. 52071227), Key Scientific Research Project in Shanxi Province (Grant No. 201805D121003), Special Found Projects for Central Government Guidance to Local Science and Technology Development, Science and Technology Major Projects of Shanxi Province (20191102004), Natural Science Foundation of Shanxi Province of China (2019D111102), Research Project Supported by Shanxi Scholarship Council of China (HGKY2019085).

Appendix A. Supplementary data

Supplementary material related to this article can be found, in the online version, at doi:https://doi.org/10.1016/j.corsci.2021.109378.

References

[1] P. Knochel, A flash of magnesium, Nat. Chem. 1 (2009), 740–740.
[2] T.M. Pollock, Weight loss with magnesium alloys, Science 328 (2010) 986–987.
[3] M. Esmaily, J.E. Svensson, S. Fajardo, N. Birbilis, G.S. Frankel, S. Virtanen, R. Arrabal, S. Thomas, L.G. Johansson, Fundamentals and advances in magnesium alloy corrosion, Prog. Mater. Sci. 89 (2017) 92–193.
[4] G.S. Frankel, Magnesium alloys: ready for the road, Nat. Mater. 14 (2015) 1189–1190.
[5] G.L. Song, A. Atrens, Corrosion mechanisms of magnesium alloys, Adv. Eng. Mater. 1 (1999) 11–33.
[6] D. Lu, X. Ma, Y. Huang, F. Ma, J. Duan, B. Hou, Surface alloying of a magnesium alloy with zinc oxide by taking advantage of the permeability of the magnesium oxide film, J. Phys. Chem. C 123 (2019) 24461–24468.
[7] Y. Chen, S. Zhao, B. Liu, M. Chen, J. Mao, H. He, Y. Zhao, N. Huang, G. Wan, Corrosion-controlling and osteo-compatible Mg ion-integrated phytic acid (Mg-PA) coating on magnesium substrate for biodegradable implants application, ACS Appl. Mater. Interfaces 6 (2014) 19531–19543.
[8] B. Zhang, R. Yao, L. Li, Y. Wang, R. Luo, L. Yang, Y. Wang, Green tea polyphenol induced Mg^{2+}-rich multilayer conversion coating: toward enhanced corrosion resistance and promoted in situ endothelialization of AZ31 for potential cardiovascular applications, ACS Appl. Mater. Interfaces 11 (2019) 41165–41177.

[9] Y. Yang, J. Zhou, Q. Chen, R. Detsch, X. Cui, G. Jin, S. Virtanen, A.R. Boccaccini, In vitro osteocompatibility and enhanced biocorrosion resistance of diammonium hydrogen phosphate-pretreated/poly (ether imide) coatings on magnesium for orthopedic application, ACS Appl. Mater. Interfaces 11 (2019) 29667–29680.
[10] H. Yang, X. Guo, X. Chen, N. Birbilis, A homogenisation pre-treatment for adherent and corrosion-resistant Ni electroplated coatings on Mg-alloy AZ91D, Corros. Sci. 79 (2014) 41–49.
[11] S. Moon, Y. Nam, Anodic oxidation of Mg–Sn alloys in alkaline solutions, Corros. Sci. 65 (2012) 494–501.
[12] C. Zhang, L. Wu, H. Liu, G. Huang, B. Jiang, A. Atrens, F. Pan, Microstructure and corrosion behavior of Mg-Sc binary alloys in 3.5 wt.% NaCl solution, Corros. Sci. 174 (2020), 108831.
[13] M. Yin, L. Hou, X. Liu, Z. Wang, B. Liu, J. Jia, S. Zhang, Y. Wei, Tailoring the micromorphology of the as-cast Mg-Sn-In alloys to corrosion-resistant microstructures via adjusting in concentration, J. Alloys. Compd. 811 (2019), 152024.
[14] L. Hou, N. Dang, H. Yang, B. Liu, Y. Li, Y. Wei, X.B. Chen, A combined inhibiting effect of sodium alginate and sodium phosphate on the corrosion of magnesium alloy AZ31 in NaCl solution, J. Electrochem. Soc. 163 (2016) C486–C494.
[15] G.L. Song, A. Ataens, X.L. Wu, B. Zhang, Corrosion behaviour of AZ21, AZ501 and AZ91 in sodium chloride, Corros. Sci. 40 (1998) 1769–1791.
[16] J. Yang, J. Peng, E.A. Nyberg, F.S. Pan, Effect of Ca addition on the corrosion behavior of Mg-Al-Mn alloy, Appl. Surf. Sci. 369 (2016) 92–100.
[17] W. Xu, N. Birbilis, G. Sha, Y. Wang, J.E. Daniels, Y. Xiao, M. Ferry, A high-specific-strength and corrosion-resistant magnesium alloy, Nat. Mater. 14 (2015) 1229–1235.
[18] L. Hou, M. Raveggi, X.B. Chen, W. Xu, K.J. Laws, Y. Wei, M. Ferry, N. Birbilis, Investigating the passivity and dissolution of a corrosion resistant Mg-33at.%Li alloy in aqueous chloride using online ICP-MS, J. Electrochem. Soc. 163 (2016) C324–C329.
[19] N. Birbilis, G. Williams, K. Gusieva, A. Samaniego, M.A. Gibson, H.N. McMurray, Poisoning the corrosion of magnesium, Electrochem. Commun. 34 (2013) 295–298.
[20] J. Yang, C.D. Yim, B.S. You, Characteristics of surface films formed on Mg-Sn alloys in NaCl solution, J. Electrochem. Soc. 163 (8) (2016) C395–C401.
[21] T.W. Cain, C.F. Glover, J.R. Scully, The corrosion of solid solution Mg-Sn binary alloys in NaCl solutions, Electrochim. Acta 297 (2019) 564–575.
[22] J. Yang, C.D. Yim, B.S. You, Effects of Sn in α-Mg matrix on properties of surface films of Mg-xSn (x = 0, 2, 5 wt%) alloys, Mater. Corros. 67 (2016) 531–541.
[23] H.Y. Ha, J.Y. Kang, J. Yang, C.D. Yim, B.S. You, Role of Sn in corrosion and passive behavior of extruded Mg-5 wt%Sn alloy, Corros. Sci. 102 (2016) 355–362.
[24] J. Wang, Y. Li, S. Huang, X. Zhou, Study of the corrosion behavior and the corrosion films formed on the surfaces of Mg-xSn alloys in 3.5wt.% NaCl solution, Appl. Surf. Sci. 317 (2014) 1143–1150.
[25] E. Brandes, G. Brook, Smithells Metals Reference Book, Butterworth-Heinemann, 1983.
[26] S. Yuan, H. Lu, Z. Sun, L. Fan, X. Zhu, W. Zhang, Electrochemical performance of Mg-3Al modified with Ga, in and Sn as anodes for Mg-air battery, J. Electrochem. Soc. 163 (2016) A1181–a1187.
[27] J. Li, B. Zhang, Q. Wei, N. Wang, B. Hou, Electrochemical behavior of Mg-Al-Zn-In alloy as anode materials in 3.5 wt.% NaCl solution, Electrochim. Acta 238 (2017) 156–167.
[28] N. Wang, R. Wang, C. Peng, B. Peng, Y. Feng, C. Hu, Discharge behaviour of Mg-Al-Pb and Mg-Al-Pb-In alloys as anodes for Mg-air battery, Electrochim. Acta 149 (2014) 193–205.
[29] H. Xiong, L. Li, Y. Zhang, K. Yu, H. Fang, Y. Dai, H. Dai, Microstructure and discharge behavior of Mg-Al-Sn-In anode alloys, J. Electrochem. Soc. 164 (2017) A1745–A1754.
[30] P. Gore, T.W. Cain, J. Laird, J.R. Scully, N. Birbilis, V.S. Raja, Enrichment efficiency of noble alloying elements on magnesium and effect on hydrogen evolution, Corros. Sci. 151 (2019) 206–218.
[31] A. Sadeghi, E. Hasanpur, A. Bahmani, K.S. Shin, Corrosion behaviour of AZ31 magnesium alloy containing various levels of strontium, Corros. Sci. 141 (2018) 117–126.
[32] P.P. Wu, F.J. Xu, K.K. Deng, F.Y. Han, Z.Z. Zhang, R. Gao, Effect of extrusion on corrosion properties of Mg-2Ca-χAl (χ = 0, 2, 3, 5) alloys, Corros. Sci. 127 (2017) 280–290.
[33] Z. Hu, X. Li, Q. Hua, H. Yan, H.X. Qiu, X.M. Ruan, Z.H. Li, Effects of Sm on microstructure and corrosion resistance of hot-extruded AZ61 magnesium alloys, J. Mater. Res. 30 (2015) 3671–3681.
[34] Z. Yin, Y. Chen, H. Yan, G.H. Zhou, X.Q. Wu, Z. Hu, Effects of the second phases on corrosion resistance of AZ91-xGd alloys treated with ultrasonic vibration, J. Alloys. Compd. 783 (2019) 877–885.
[35] A.J. Forty, Corrosion micromorphology of noble metal alloys and depletion gilding, Nature 282 (1979) 597–598.
[36] A.J. Forty, P. Durkin, A micromorphological study of the dissolution of silver-gold alloys in nitric acid, Philos. Mag. A 42 (2006) 295–318.
[37] P. Durkin, A.J. Forty, Oxide formation during the selective dissolution of silver from silver-gold alloys in nitric acid, Philos. Mag. A 45 (2006) 95–105.
[38] G.W. Akimov, Electrode potentials (Part 1 of 2 Parts), Corrosion 11 (11) (1955) 31–40.
[39] G.W. Akimov, Electrode potentials (Part 2 of 2 Parts), Corrosion 11 (12) (1955) 27–46.
[40] B. Vanrenterghem, A. Papaderakis, S. Sotiropoulos, D. Tsiplakides, S. Balomenou, S. Bals, T. Breugelmans, The reduction of benzylbromide at Ag-Ni deposits prepared by galvanic replacement, Electrochim. Acta 196 (2016) 756–768.
[41] P. Gore, S. Fajardo, N. Birbilis, G.S. Frankel, V.S. Raja, Anodic activation of Mg in the presence of In^{3+} ions in dilute sodium chloride solution, Electrochim. Acta 293 (2019) 199–210.